Applied Catalysis B: Environmental 152–153 (2014) 117–128

Contents lists available at ScienceDirect

Applied Catalysis B: Environmental

journal homepage: www.elsevier.com/locate/apcatb

The effect of catalyst modification on the conversion of glycerol to allyl alcohol

G. Sánchez, J. Friggieri, C. Keast, M. Drewery, B.Z. Dlugogorski, E. Kennedy, M. Stockenhuber*

Priority Research Centre for Energy (PRCfE), The University of Newcastle, Callaghan, NSW 2308, Australia

ARTICLE INFO

Article history:
Received 5 July 2013
Received in revised form
23 December 2013
Accepted 13 January 2014
Available online 23 January 2014

Keywords:
Glycerol conversion
Allyl alcohol
Acrolein
Alkali metal modification
γ-Alumina

ABSTRACT

Conversion of glycerol to allyl alcohol was carried out over an iron on alumina catalyst. With the aim of enhancing selectivity towards the desired product and to reduce acrolein formation (a detrimental impurity in the subsequent epoxidation of allyl alcohol) the supported iron catalyst was modified using alkali metals. It was found that lithium, sodium, potassium, rubidium and caesium deposition on the catalyst surface increased allyl alcohol yield and reduced the rate of catalyst deactivation. Coincidently, acrolein selectivity decreased by up to 75% following treatment with the alkali salt.

Changes in the product distribution were determined to be associated with altering the acid/base properties of the catalyst, as confirmed by isopropanol dehydration/dehydrogenation, ammonia and carbon dioxide temperature programmed desorption. The treatment was also found to influence the physical properties of the catalyst surface. A correlation between acid to basic site concentration and allyl alcohol selectivity was established. A reduction in the former value results in an enhancement in the rate of allyl alcohol formation. A reaction mechanism was developed based on the effect of iron and alkali metals catalysing the conversion of glycerol into allyl alcohol. The proposed catalyst modification technique is a straightforward method, readily applicable at a larger scale due to the simplicity of the alkali inclusion and its striking influence on the reaction selectivity.

1. Introduction

Global concern over carbon dioxide emissions and the exhaustion of fossil fuel resources make the development of synthetic fuels a field of intense study, facilitating the development of industrial applications of reactions such as the transesterification of triglycerides [1,2]. Although the transesterification of triglycerides is the most widely adopted biodiesel production method, it invokes the necessity to deal with glycerol, a by-product formed during the reaction [1]. In biodiesel production through transesterification, glycerol formation has serious implications for manufacturers, accounting for approximately 10 wt% of the product generated [3]. Despite its multiple uses, the purification of the fatty-acid methyl esters (FAME) by-product (containing from 30 to 60 wt% of the trivalent alcohol [4]) to the level of purity required for sale entails costly and specialised techniques. Additionally, markets for glycerol are considered to be saturated and therefore unable to accommodate the large quantities of crude glycerol being produced. In 2005, 200,000 tonnes of glycerol were generated as part of the biodiesel manufacturing process, while demand for refined glycerol was roughly 900,000 tonnes. In 2008, the rate of glycerol generated from transesterification increased to 1.224 million tonnes, with no reported parallel growth in glycerol markets [5]. Consequently, the commercial value of glycerol has dropped, adding significant cost to biodiesel manufacturers for storage and appropriate disposal. Clearly, finding a suitable glycerol derivative, with a significant market demand and price is essential, with glycerol valorisation to enhance the viability of the biodiesel manufacturing process.

Crude glycerol currently represents a waste (and therefore a financial liability) for the biodiesel industry, however it is a low cost reactant for which a number of technological options are currently being explored. While one of these options is the production of acrolein [6], a more valuable conversion product is allyl alcohol, which has a 36% higher market value [7]. Allyl alcohol global production was estimated to be 136,000 tonnes in 2005 [8]. It is also possible to convert allyl alcohol to products of higher value such as glycidol, which has a current market price of US$546 per kilogram [7]. This potential opportunity makes pathways towards allyl alcohol production of considerable interest. Due to the bi-functionality (hydroxyl group and carbon–carbon double bond) of the molecule,

* Corresponding author. Tel.: +61 0249854433.
E-mail address: michael.stockenhuber@newcastle.edu.au (M. Stockenhuber).

0926-3373/$ – see front matter © 2014 Elsevier B.V. All rights reserved.
http://dx.doi.org/10.1016/j.apcatb.2014.01.019

allyl alcohol is often used as a chemical intermediate. As reported by others [9], conversion of glycerol to allyl alcohol can be achieved over iron catalysts in a two-step process (acrolein formation followed by the selective hydrogenation of the double bond in acrolein promoted by glycerol or/and other alcohols). The role of iron in the process remains uncertain.

The direct conversion of glycerol to allyl alcohol has been reported over bimetallic catalysts (zirconia-iron surfaces) [10] or using formic acid as a reactant, which causes glycerol to undergo a double dehydroxylation [11]. Other catalysts such as a MoO_3–WO_3/TiO_2 [12] and methyltrioxorhenium (MTO) [13] have also been found to selectively catalyse allyl alcohol formation from glycerol.

Glycerol conversion to acrolein was achieved over acidic zeolites, with selectivities of up to 70% being reported [14]. Catalyst acidity influences both selectivity and conversion. A Hammett acidity value between −8.2 and −3.0 [15,16] was suggested to be ideal for the conversion of glycerol into the aldehyde. Low selectivity or accelerated deactivation were observed over catalysts with acid strengths outside this range [3]. Conversely, allyl alcohol as main product has been obtained using surfaces of very weak acidity, such as zirconia-supported iron oxide [10]. Clearly the product distribution of the converted glycerol is expected to be strongly dependent on the acid and base properties of the catalyst and or support.

Porous alumina is extensively used as a catalyst support in industrial processes due to its high surface area and minimal transport limitations. The γ phase of alumina is slightly acidic but it is possible to neutralise it through deposition of alkali metals [17]. In addition to the influence on surface acidity, alkali metals were reported to induce structural alterations on the catalyst, and thus improving iron dispersion for supported iron catalysts [18]. The electronic effects of alkali metals also can influence the catalyst activity [18]. This has been attributed to either ion exchange of alkali cations with protons from surface hydroxyl groups present in γ alumina, or the interaction of the introduced cation and anion with the Lewis acidic aluminium sites [19]. Various characterisation techniques, including IR spectroscopy, indicators with different pK_a, X-ray photoelectron spectroscopy and temperature programmed desorption, have been applied to determine the nature and distribution of the active sites being modified. While implications on the effect of total surface acidity have been observed, some authors attribute changes to the removal of Lewis sites, others to the replacement of Brønsted acidity or even a combination of the two [20]. The catalytic activity/selectivity is said to be related to the ionic radii of the modifier [21]. However, the catalyst modification is not necessarily straightforward, as under some conditions the effect on acid concentration or strength is unexpected. Furthermore, not only the nature of the alkali cation is important for the acid base properties but also the concentration of the solution used to treat the support [19]. Structural properties were also altered by alkali metal modification as indicated by inhibition of iron cluster formation due to Rb. Rubidium was used to modify iron oxide on silica catalysts, and inhibited cluster modification by parallel ion exchange between the iron and the added alkali cation [18]. Alkali metal-supported zirconia-iron oxide catalysts were reported to improve allyl alcohol production and reduce the concentration of some reaction by-products [22].

In this work, we aim to use alkali metal deposition techniques to modify iron surfaces prepared by a novel non-aqueous impregnation method and study its effect on the direct catalytic conversion of glycerol to allyl alcohol. It was the intention to increase selectivity to allyl alcohol, and minimise the formation of acrolein in the conversion of glycerol, since in the course of the allyl alcohol epoxidation to glycidol, acrolein competes with the alcohol, consuming peroxide and forming other species instead of the desired glycidol [23]. Reduction of acrolein formation in the upstream process is clearly preferred to purification in a separate step. Alkali metals are present in crude glycerol from biodiesel manufacturing [24] (when the reaction is base catalysed, present in the resultant mixture as waste catalyst up to 10% or as low as 0.05% after purification [25]), and thus could potentially aid the process through improved selectivity/yield. A detailed understanding of alkali metal modification is necessary to determine the economically most viable process conditions of glycerol conversion to value added products.

2. Experimental

2.1. Catalyst preparation

All materials were synthesised by a recently developed non-aqueous impregnation method. High purity alumina spheres (Sasol 1,8/210) were dehydrated for 1 h at 120 °C. Similarly, $CaSO_4{\cdot}2H_2O$ (99% Sigma Aldrich) was heated at 220 °C for 2 h to obtain the anhydrous form. The precursor salt, $Fe(NO_3)_3{\cdot}9H_2O$ (98% Sigma Aldrich), was dissolved in methanol and the solution was dried using $CaSO_4$. The resultant suspension was filtered under vacuum and the spheres added to the filtrate. After allowing the solvent to evaporate under continuous stirring, the catalyst was calcined in air for 4 h at 400 °C. The alkali metal treatment was accomplished following calcination.

Different methods were implemented for rubidium deposition on the iron oxide catalyst surface. Catalysts were modified by rinsing the spheres (washing), impregnation or ion exchange with $RbNO_3$. Impregnation consisted in adding the iron catalyst to a 0.1 M solution of rubidium nitrate in water, allowing the solution to evaporate under continuous stirring. For ion exchange, the iron on alumina catalyst was added to a fresh solution of rubidium nitrate in water stirring it overnight at 50 °C. The catalyst was then filtered and the treatment was repeated two more times. All the techniques investigated showed advantages and disadvantages, with impregnation and ion exchange allowing greater control of the quantity of modifier, while washing did not allow accurate control of modifier concentration in the solid product. Inductively coupled plasma atomic emission spectroscopy was used to determine the final catalyst composition. The influence of the sequence of metal impregnation on catalyst properties was also studied. "Inverse treatment" is described as the impregnation of rubidium (by ion exchange) being conducted prior to addition of active iron phase. In order to investigate the effect of the modifiers, Li, Na, K, Rb and Cs modified catalysts were prepared. Solutions of sodium nitrate and potassium nitrate (0.1 M) in methanol and lithium nitrate and caesium nitrate (0.1 M) in water were used to wash the spheres. The catalysts were then dried at room temperature.

2.2. Catalyst characterisation

Surface areas of used and fresh catalysts, both treated and untreated, were determined by nitrogen adsorption. The materials were first degassed overnight under vacuum and at 150 °C using a Micromeritics Vac Prep 061 sample preparation device. Tests were carried out in a Micromeritics Gemini surface area analyser at −196 °C and based on these data, Langmuir surface areas were calculated. X-ray diffraction measurements were conducted on unmodified and modified catalysts fresh and used using a Phillips X'pert Pro diffractometer with Cu Kα incident radiation (λ = 1.54060 Å). Thermogravimetric studies were carried out for unmodified and rubidium modified iron catalyst using a Metter Toledo TGA/DSC 1 apparatus. Data was collected using 8.0 mg of sample at a heating rate of 5 °C min^{-1} with a nitrogen flow of approximately 20 cm^3 min^{-1}. XPS spectra were obtained by means of a Thermo Scientific ESCALAB 250Xi electron

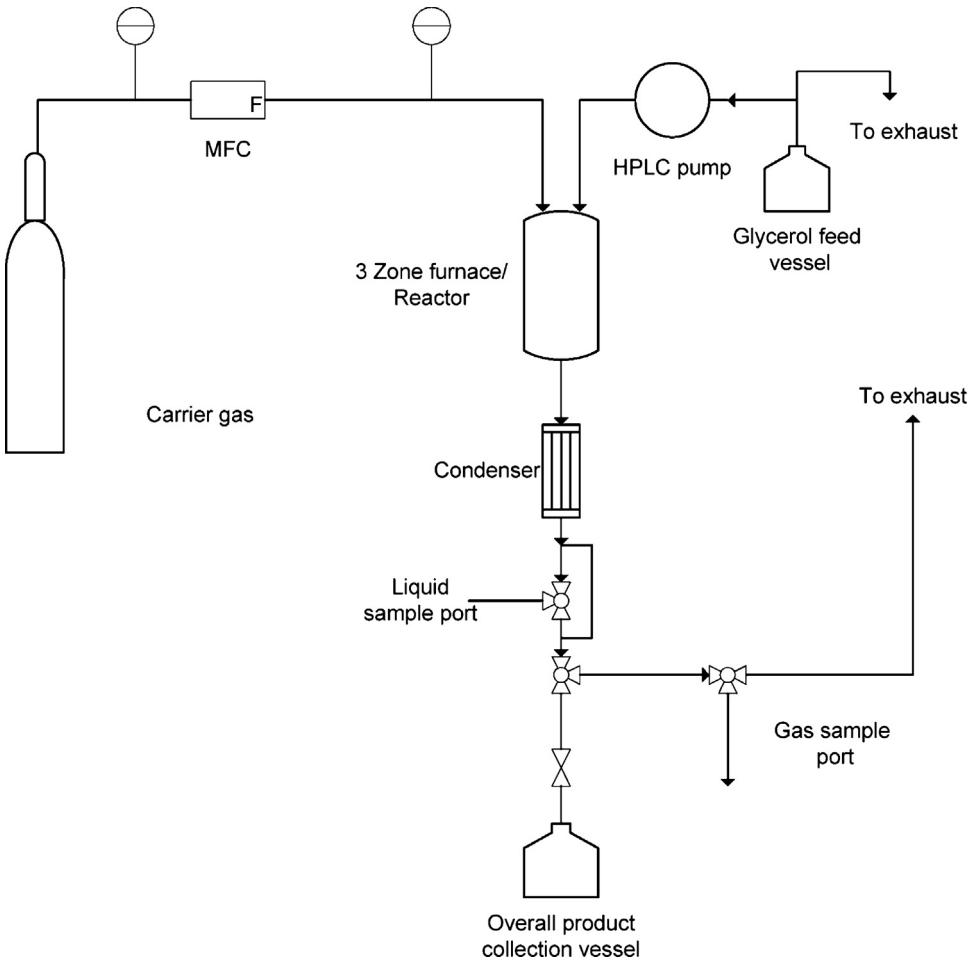

Fig. 1. Experimental setup.

spectrometer equipped with a mono-chromatic Al K alpha X-ray source (energy = 1486.68 eV). Preceding experiments, the spectrometer was calibrated using the following binding energies: Au 4f7 = 83.96 eV, Ag 3d5 = 368.21 eV and Cu 2p3 = 932.62 eV. Infrared spectra were recorded using a Bruker Tensor 27 running with an OPUS software. Samples were pressed into disks and the data collected with a resolution of 4 cm^{-1}.

Temperature programmed desorption (TPD) experiments were conducted under high vacuum in a stainless steel apparatus described before [26]. The analysis of the gas phase was carried out by a Pfeiffer Prisma quadrupole mass spectrometer. Samples were activated in the desorption cell at 400 °C. Isopropanol was adsorbed at 80 °C, then desorption of gas phase products was measured by mass spectrometry analysis as a function of temperature between 30 °C and 800 °C at a heating rate of 5 °C min^{-1}. m/z = 58 and m/z = 42 were used in analyses for acetone and propylene respectively. In a separate set of experiments, ammonia was adsorbed at 150 °C following activation and the desorption test was undertaken between 30 °C and 400 °C with a heating rate of 5 °C min^{-1}. For NH_3 analysis, m/z = 16 was used, as a constant 7% contribution attributable to water was determined for this m/z ion current. For quantitative analysis, calibration curves were prepared using Z-SM5, Si/Al = 15. Acid site density was calculated using the following equation:

$$D_s = \frac{n_{ads}}{m \cdot SA} \quad (1)$$

where D_s: site density (mmol m^{-2}); n_{ads}: moles of adsorbate desorbed from the catalyst surface (mmol); m: sample mass (g); SA: specific surface area (m^2 g).

Carbon dioxide was adsorbed at 115 °C following activation and desorption tests were conducted between 30 °C and 400 °C with a heating rate of 5 °C min^{-1}. For quantitative analysis, calibration curves were prepared decomposing $NaHCO_3$. Basic site density was calculated through Eq. (1).

2.3. Catalytic measurements

Catalytic reactions were conducted in a vertical packed bed reactor at atmospheric pressure. A Labec HTF 40 three zone electrical furnace with an operating range between 20 °C and 1200 °C was employed, with temperatures measured at the centre of the catalyst bed. A HPLC pump (Kontron Instruments 422) was used to feed the reactant mixture (glycerol 35 wt% aqueous solution) through a preheater. Nitrogen was introduced as carrier gas by means of a Brooks 5850E mass flow controller at a volumetric flow of 226 cm^3 min^{-1}. The setup was equipped with a condenser and sampling port, allowing liquid product to accumulate and samples to be taken at regular intervals for analysis. It was possible to estimate the recovery in the liquid phase. The overall product was collected in a sealed vessel (Fig. 1). Experiments were carried out at 340 °C.

For liquid phase product analysis, samples were diluted in methanol and cyclohexanone (99.8% Sigma Aldrich) was added as internal standard. Product analysis was carried out by gas chromatography, performed using an Agilent 6890 Series GC System equipped with an Agilent 5973N Mass Selective Detector (MS) and a Restek Rtx wax 30 m 0.32 mm ID, 1 μm film thickness column. For quantification, gas chromatography was also employed using

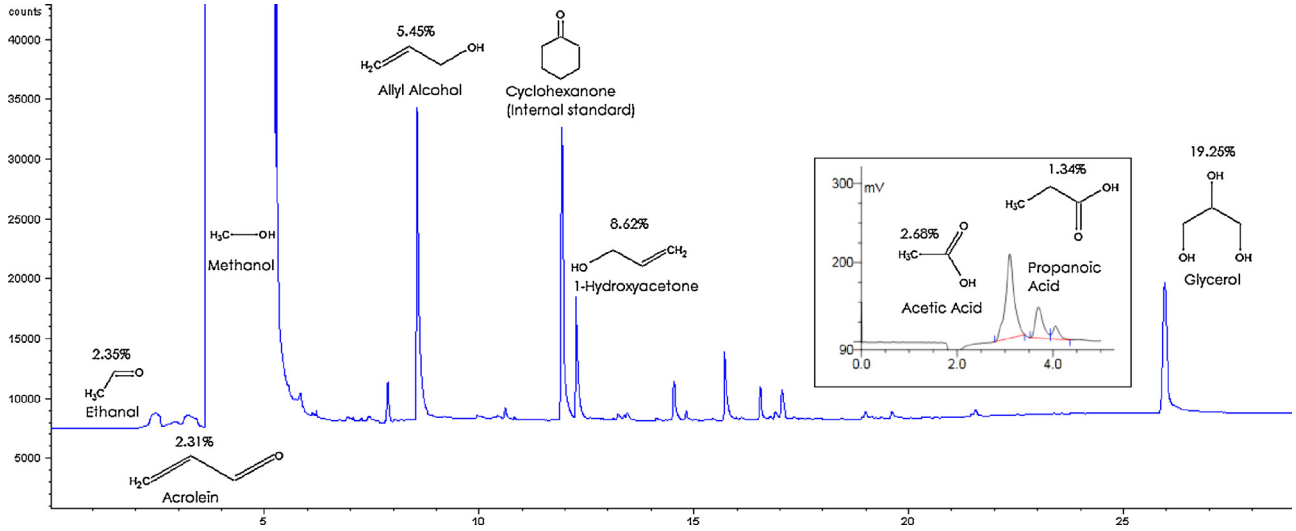

Fig. 2. Species yield, GC-FID and IC traces for a typical run over the iron catalyst. Temperature: 340 °C. Reactant: 35 wt% glycerol aqueous solution. GHSV = 1190 h^{-1}.

a HP 5890A model GC, equipped with a flame ionisation detector (FID) and a Restek Stabilwax 30 m 0.32 mm ID 1 μm film thickness column. For these analyses, the split ratio was 100:1. The injector temperature was 300 °C, detector temperature 320 °C, oven initial temperature 35 °C (for 5 min), followed by a heating at a rate of 10 °C min^{-1} to 200 °C and holding this temperature for 20 min. Detection and quantification of organic acids was undertaken by Ion Chromatography (IC) using a Suppressed Conductivity Detector on a Dionex DX-100 equipped with an Ionpac CS12 analytical column.

The gas phase was analysed using an IR Prestige 21 Shimadzu FTIR QP 5000 apparatus in conjunction with a Varian 490-GC micro gas chromatograph that allowed both product identification and quantitative analyses.

3. Results and discussion

3.1. Experiments over unmodified catalysts

A solution of 35 wt% glycerol in water was mixed (GHSV of approximately 1190 h^{-1}) with nitrogen carrier gas (226 cm^3 min^{-1}) at 340 °C over an unmodified iron oxide on alumina catalyst. This resulted in the formation of allyl alcohol, acrolein, ethanal, hydroxyacetone, acetic acid and propanoic acid as main reaction liquid products, with approximately 95% total mass recovery (Fig. 2). Using unmodified iron oxide on alumina catalysts, 42% of the carbon was accounted for, whereas, products generated over modified surfaces resulted in 60% of the total elemental balance. However, following a similar procedure as described before [9], the sum of quantified and unquantified peak areas results in approximately 91% of the carbon balance.

Blank experiments were conducted over the catalyst support, in the absence of iron, under the same conditions as outlined above. Product distribution and conversion values obtained on this surface (Table 1) are in good agreement with previous studies over similar materials, in which complete conversion of glycerol was observed [27]. The activity of the catalyst remained relatively constant for five hours. Problems with product desorption (typical of a strongly acidic catalyst) are not observed, even on the unmodified alumina, presumably due to its moderate acidity [27]. It is evident from Table 1, that the presence of iron on the catalyst is increasing allyl alcohol selectivity, which is consistent with the studies of other researchers [9,10]. In line with the literature [27], γ alumina is active in facilitating acrolein formation at relatively high selectivities. Iron appears to form sites that catalyse the conversion of glycerol to allyl alcohol and simultaneously remove sites that are responsible for acrolein formation.

Table 1
Comparison of product distribution obtained over the iron catalyst and its support.

Product	γ-Alumina/Fe	γ-Alumina
Allyl alcohol yield (%)	4.3	1.5
Acrolein selectivity (%)	4.3	14.5
Glycerol conversion (%)	78.8	99.8

Experiments were undertaken, by reducing the catalyst weight by 90% (and thus the GHSV), resulting in relatively low conversion of glycerol in order to identify the primary products in the reaction. At glycerol conversion levels of 35–40%, the hydroxyacetone yield was 4%. Conversely, ethanal production was significantly lower (Fig. 3) compared to conditions where the glycerol conversion was high. This implies that ethanal is a secondary product of the reaction, which formation depends on the production of an intermediate generated at sufficient concentrations only at higher glycerol conversion levels. In a related study of the dehydration of glycerol to vinyl alcohol, formaldehyde has been reported [12], with vinyl alcohol undergoing tautomerism to yield ethanal. The intermediate vinyl alcohol/formaldehyde step could result in an inverse relationship developed between selectivity and GHSV. Vinyl alcohol is suggested to be a potential intermediate in the conversion of glycerol to ethanal. We did not detect formaldehyde under our

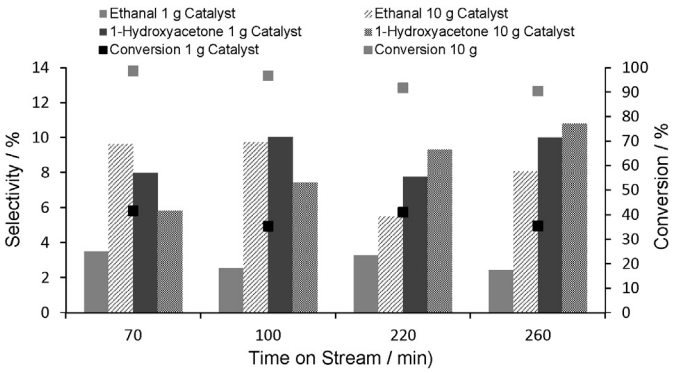

Fig. 3. Catalytic measurements running at moderate conversions. Reactant: 35 wt% glycerol aqueous solution. Temperature: 340 °C. GHSV = 119 h^{-1}.

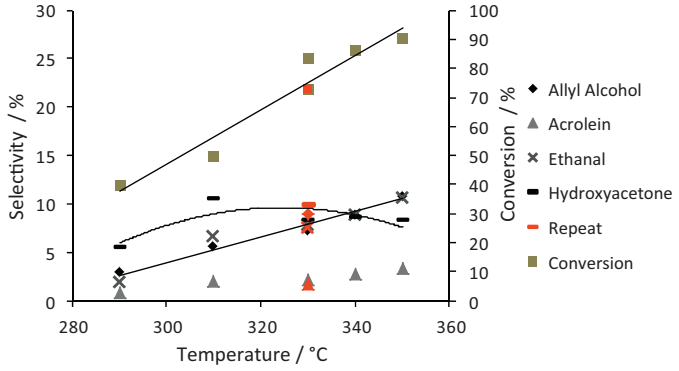

Fig. 4. Product distribution as a function of the reaction temperature. Reactant: 35 wt% glycerol aqueous solution. Catalyst: unmodified iron oxide on alumina.

reaction conditions as formaldehyde is likely to decompose to hydrogen and carbon monoxide, as reported previously [12,28].

In order to gain further insight into the reaction mechanism, a solution of 17.5 wt% acrolein in water was fed into the reactor under the same conditions using an unmodified iron oxide catalyst. In these studies, very low concentrations of hydroxyacetone and allyl alcohol (0.08% and 0.1% yield, respectively) were observed, while the concentration of ethanal, in both liquid and gas samples, was relatively high (7.2% for a 67.5% acrolein conversion). In the light of these findings, two conclusions can be drawn; first it is apparent that there is a direct pathway for ethanal formation, in addition to the pathway involving 1,3 glycerol dehydration, and the subsequent decomposition to vinyl alcohol and formaldehyde. Secondly, acrolein formation does not lead to allyl alcohol production. Under the conditions examined in the present study, acrolein is not hydrogenated over the iron catalyst to form allyl alcohol where a sacrificial reductant or alcohol was absent. However, hydrogen transfer to acrolein has been reported in the presence of glycerol [9]. We suggest that hydrogenation/reduction is a crucial step in the formation of allyl alcohol from glycerol.

Reaction temperature is expected to play a key role for activity and selectivity in glycerol conversion. Preliminary experiments were carried out, aiming to optimise process conditions in order to maximise the yield of allyl alcohol. Fig. 4 shows the conversion of glycerol and selectivity towards the main reaction products as a function of temperature. A repeat analysis of the data at 340 °C shows good reproducibility. This also suggests that catalyst deactivation is minimal, even after several hours of time on stream. An increase in both conversion and selectivity towards the desired product with increasing temperature was observed. In contrast, hydroxyacetone selectivity decreased at temperatures higher than 310 °C. Hydroxyacetone formation involves ionic pathways which are not dominant at high temperatures [27]. Carbon–carbon bond cleavage have been reported to occur in hydroxyacetone under similar reaction conditions to form ethanal [29], which explains the decrease in hydroxyacetone selectivity. Indications of competitive pathways leading to formation of acrolein and hydroxyacetone have been suggested by others [12].

3.2. Catalyst modification

Assessment of the efficacy of the synthesis procedures was based on allyl alcohol yield. Iron(III) salts form hydroxo species in aqueous solution depending on the pH. "Naked" Fe^{3+} cations are stable in water at very low pH values (below pH = 1). Extended iron clusters, which are preferably formed from hydroxide precipitates, are less catalytically active than small iron oxide clusters for redox reactions and acid–base reactions [30]. Materials treated by washing were observed to be more selective for allyl alcohol production (Fig. 5a), since iron was not removed by the modification. As mentioned previously, iron catalyses allyl alcohol formation, however following ion exchange with alkali metals, the concentration of the active iron phase was reduced, as determined by ICP analysis. The addition of rubidium prior to iron addition to the alumina support blocked sites available for iron deposition, resulting in a decrease in allyl alcohol selectivity on these catalysts (Fig. 5a). Other authors have reported similar findings, and observed selectivities of approximately 90% to acrolein over caesium and rubidium doped silicotungstic acid (Cs/STA and Rb/STA) supported on gamma alumina (10 wt% aqueous glycerol solution [28]). Glycerol conversions of up to 100% were observed over rubidium on alumina catalysts, which is in agreement with previous studies with Cs/STA and Rb/STA, where catalyst stability was enhanced after supporting these materials on alumina [28]. Differences in the level of catalyst deactivation over surfaces synthesised either by impregnation or ion exchange of the alkali metal (75.4% and 98.7% glycerol conversion respectively after three hours of catalytic tests) were thought to be a consequence of differences in the level of iron dispersion resulting from the impregnation process. For impregnation techniques, the alkali cations are believed to create an unknown dispersion on the catalyst, which poisons some of the active iron sites, whereas ion exchange preferably occurs on unsaturated sites of the iron catalyst. Washing and inverse synthesis resulted in relatively stable catalysts, with the conversion of glycerol reaching 90% after four hours of time on stream.

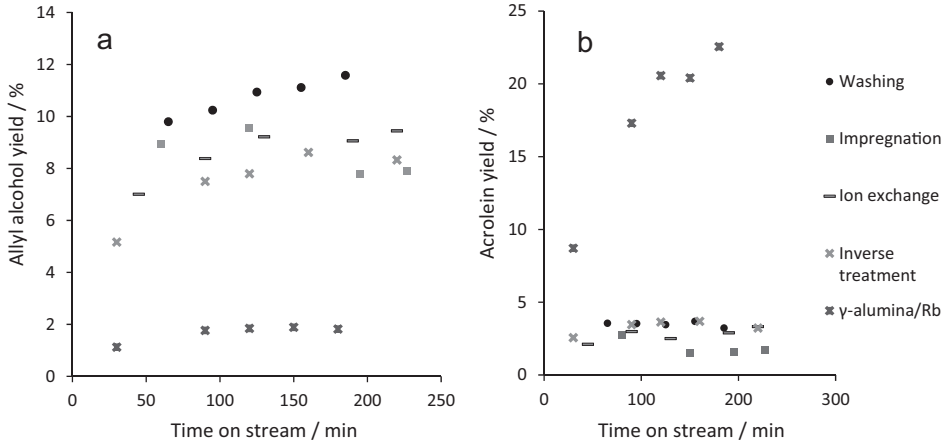

Fig. 5. (a) Allyl alcohol yield as a function of time on stream. (b) Acrolein yield as a function of time on stream. Modifier: rubidium. Temperature: 340 °C. Reactant: 35 wt% glycerol aqueous solution. GHSV = 1190 h^{-1}.

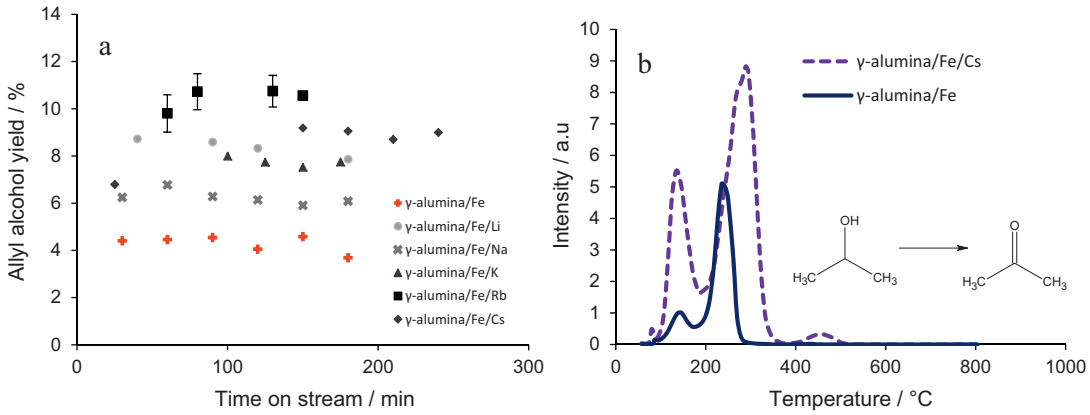

Fig. 6. (a) Effect of catalyst treatment on allyl alcohol yield as a function of time on stream with glycerol conversion at 340 °C. Reactant concentration: 35 wt%. GHSV = 1190 h^{-1} [31]. (b) Isopropanol desorption on the surface of treated and unmodified catalysts. m/z = 58 (acetone).

3.3. Acid basic properties of modified catalysts

Rinsing the iron catalysts with alkali solutions resulted in the formation of catalysts with the highest selectivity towards allyl alcohol. Each modifier (lithium, sodium, potassium, rubidium and caesium) was incorporated (in batches) on the iron oxide catalyst using the washing technique. For characterisation of the acid base properties of the catalyst, isopropanol (IPA) adsorption was used, as described in [18]. IPA decomposition product analysis enables a particular catalyst to be assessed in terms of whether the catalyst will act as an acid or a base in the reaction.

It is generally accepted that IPA dehydrogenation to acetone occurs over basic catalysts, whereas dehydration of IPA to propylene is associated with a catalyst which is acidic in nature [18]. The alkali metal treatment implemented in the current study significantly increased the basicity of the catalyst, as the IPA dehydrogenation route was favoured over caesium treated materials. Decreasing quantities of acetone were detected over unmodified catalysts, suggesting that modifiers increase the number of basic sites on the catalyst. Correspondingly, catalyst modification has a clear effect on product distribution in the conversion of glycerol (Fig. 6a). In the presence of the alkali metal salt, the yield of allyl alcohol increased from 4% to between 6% and 11% absolute, depending on the cation used as modifier.

For alkali metal salt-treated catalysts, the yield of acrolein decreased by up to 75% under some conditions, compared to an unmodified catalyst (Fig. 7b). The higher yield of propylene formed over unmodified catalysts is evidence of the neutralisation of acid sites occurring during treatment with alkali metals (Fig. 7a). Conversion of IPA dropped as a result of the alkali addition. Similar results for IPA decomposition were reported on the rubidium modification of silica supported iron oxide [18]. Selecting the alkali metal for catalyst modification with the optimum performance comprises a balance between high selectivity towards allyl alcohol, low selectivity towards acrolein and high conversion of glycerol.

To substantiate the influence of the alkali treatment on acidity and basicity, ammonia and carbon dioxide TPD experiments were undertaken. When studying the iron-based catalysts by ammonia desorption, the results are qualitatively consistent with the isopropanol test. Iron impregnation results in a reduction of the strength and number of acid sites, as shown in Fig. 8a. Moderate acidity was observed on alkali modified surfaces, as denoted by the NH_3 peaks around 130 °C and 385 °C. The alkali metals examined were found to reduce the acid site density of the iron oxide catalyst from 1.87 μmol m^{-2} to as low as 1.05 μmol m^{-2} with the rubidium modification (for calculation procedure, refer to Section 2.2). Moreover, the alkali catalyst modification affects the strength of acid sites. For lithium and caesium treated catalysts, a decrease in acid strength was evident (Table 2). The quantity of carbon dioxide adsorbed on the same surfaces was significantly lower than the values obtained from ammonia desorption. Changes in the number and strength of basic sites were observed following alkali metal modification. Basic site density increased from 0.04 μmol m^{-2} for the unmodified iron catalyst to 0.12 μmol m^{-2} for the potassium treated surface (Table 3).

Differences in the acid and basic amounts measured on alkali modified catalysts are consequences of factors such as the size of cation employed in the modification, its electronegativity and the

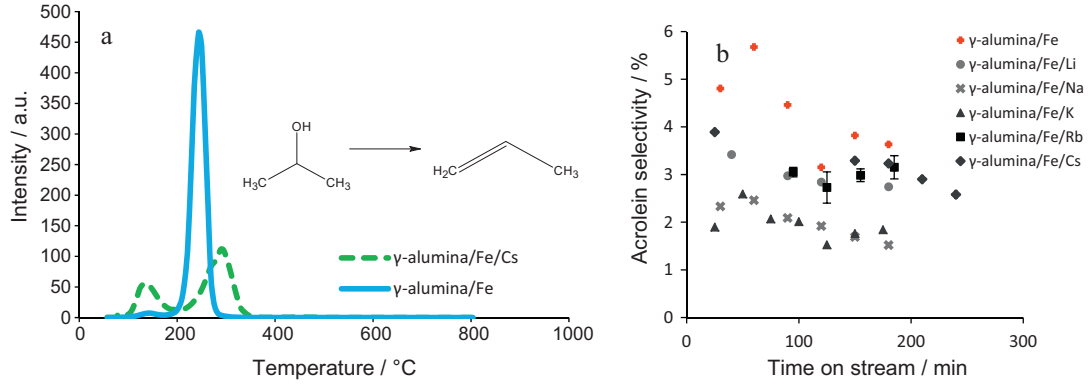

Fig. 7. (a) Isopropanol desorption on the surface of treated and unmodified catalysts. m/z = 42 (propylene). (b) Effect of catalyst treatment on acrolein selectivity as a function of time on stream with glycerol conversion at 340 °C. Reactant concentration: 35 wt%. GHSV = 1190 h^{-1}.

Table 2
Ammonia desorption over unmodified and modified catalysts.

Catalyst	Average desorption temperature (°C)	Acid site density (μmol m^{-2})	Acid site concentration (mmol g^{-1})
γ-Alumina	234	1.87	0.38
γ-Alumina/Fe	223	1.73	0.28
γ-Alumina/Fe/Na	225	1.61	0.29
γ-Alumina/Fe/Li	215	1.34	0.23
γ-Alumina/Fe/K	241	1.16	0.18
γ-Alumina/Fe/Cs	222	1.09	0.19
γ-Alumina/Fe/Rb	239	1.05	0.18

Table 3
Carbon dioxide desorption over unmodified and modified catalysts.

Catalyst	Average desorption temperature (°C)	Basic site density (μmol m^{-2})	Basic site concentration (mmol g^{-1})
γ-Alumina/Fe	154	0.04	0.007
γ-Alumina/Fe/Na	168	0.11	0.020
γ-Alumina/Fe/Li	155	0.09	0.015
γ-Alumina/Fe/K	163	0.12	0.018
γ-Alumina/Fe/Cs	154	0.07	0.012
γ-Alumina/Fe/Rb	164	0.08	0.015

Table 4
Product yields in glycerol conversion under different reaction conditions.

Catalyst	Conditions	Allyl alcohol yield (%)	Acrolein yield (%)	Conversion (%)	Reference
γ-Alumina/Fe	340 °C, WHSV^{-1} = 0.3 h, 35 wt% glycerol[a]	4.3	3.4	78.8	This study
γ-Alumina/Fe/Rb	340 °C, WHSV^{-1} = 0.3 h, 35 wt% glycerol[a]	11.6	3.2	89.8	This study
ZrO_2–FeO_x	350 °C, WHSV^{-1} = 3 h, 30 wt% glycerol[b]	13.7	6.3	100.0	[22]
Rubidium-supported ZrO_2–FeO_x	350 °C, WHSV^{-1} = 3 h, 30 wt% glycerol[b]	19.6	3.6	100.0	[22]
Fe_2O_3 ($Al(H_2PO_4)_3$ addition)	320 °C, WHSV^{-1} = 1.97 h, 35 wt% glycerol[a]	20.0	6.0	>95.0	[9]

[a] Reaction time = 3 h.
[b] Reaction time = 6 h.

change in external surface area that the treatment produces. Rubidium, caesium and potassium treated catalysts resulted in the less acidic materials. Due to steric effects, these modifiers are able to form surface alkali aluminates with less ions than the required when alkali metals with smaller atomic radius are used [19,21]. Those surface alkali aluminates neutralise the surface acidity of the alumina [19]. The particular effect of the sodium modification in acidity (Table 2) could be related to its high density which is an exception to the periodic trend in the group. This variable could influence the requirement of more mass of sodium to occupy the same volume when forming the surface alkali aluminates.

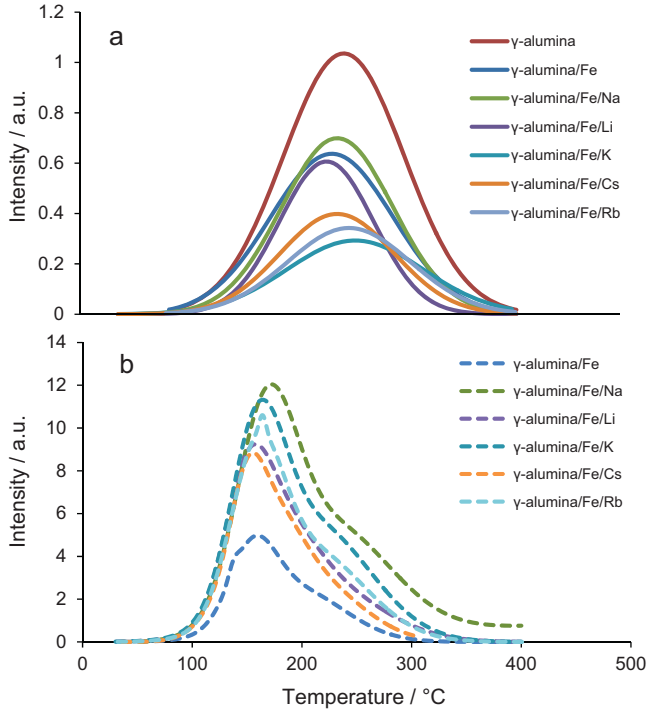

Fig. 8. (a) Ammonia desorption on the surface of modified/unmodified catalysts m/z = 16. (b) Carbon dioxide desorption on the surface of modified/unmodified catalysts m/z = 44.

Over alkali modified alumina and other supports such as zeolites, cations with low electronegativity influenced the increase in negative charge on oxygen atoms in the structure resulting in increased basicity [32,33]. Our results (Table 3) have been thought to be a consequence of stronger interactions between the adsorbate and cations with smaller atomic radius since the distances between the adsorbate and the nuclei of the (smaller) cation are shorter [32].

Correlations were established between the total acid to basic site concentration ratio and allyl alcohol and acrolein selectivity. A reduction in the former value leads to an enhanced rate of allyl alcohol formation, whereas an increase in the ratio favours acrolein production (Fig. 9b).

Table 4 shows catalytic data previously reported in glycerol conversion for comparative purposes. However an assessment is not necessarily straightforward, due to the use of different catalysts, operation at different temperatures and gas hourly space velocities, as shown. Lower allyl alcohol yields were obtained under the reaction conditions in our work compared with the work of other authors. Nevertheless, the efficacy of the alkali metal modification is clear, increasing allyl alcohol yield up to 11.6%, reducing acrolein production and helping overcoming catalyst deactivation.

3.4. Other properties of modified catalysts

Iron impregnation on the support results in a decrease in surface area. However, caustic treatment increased catalyst surface

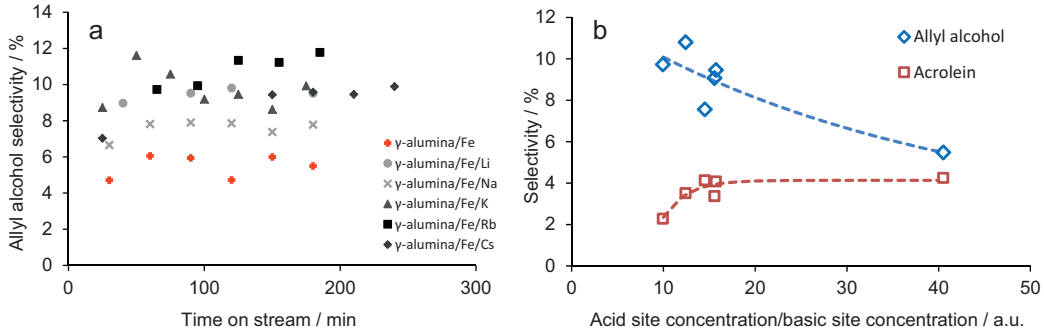

Fig. 9. (a) Effect of catalyst modification on allyl alcohol selectivity as a function of time on stream with glycerol conversion at 340 °C. Reactant concentration: 35 wt%. GHSV = 1190 h^{-1}. (b) Effect of the acid to basic site concentration ratio on selectivity towards allyl alcohol and acrolein.

Table 5
Specific surface area of alumina supported iron catalysts for glycerol conversion at 340 °C.

Catalyst	Surface area ($m^2\ g^{-1}$)
γ-Alumina	200.0
γ-Alumina/Fe fresh	164.1
γ-Alumina/Fe used	138.1
γ-Alumina/Fe/Na fresh	178.4
γ-Alumina/Fe/Na used	156.1

area by 8%, most likely a result of the removal of extraneous material present in the alumina. Higher catalyst surface areas generally lead to higher conversion levels but with lower product selectivity [12]. Subsequent to reaction, a loss in surface area for both modified and unmodified materials was observed, which has been previously associated with carbon deposition [9]. Doped catalysts exhibit a more moderate decrease in surface area than unmodified iron on alumina catalysts (Table 5). This is presumably a consequence of a reduced rate of coking which decreases the concentration of carbon in the pores of the catalyst as a result of a reduction in the acidity. These findings suggest that the alkali modification affects both, surface chemistry and surface area of the modified catalyst and in turn improves allyl alcohol selectivity and conversion.

Fig. 10 shows the diffraction patterns of unmodified catalysts, both fresh and used. Three main peaks characteristic of γ-alumina were observed which suggest high iron dispersion. Nevertheless, a hematite structure was identified in samples modified with rubidium before and following catalytic measurements (Fig. 10). The catalyst modification with rubidium seems to decrease the level of iron dispersion, enhancing crystallinity. Other authors have observed increased metal dispersion when promoting rhodium on alumina and iron on silica catalysts with alkali metals as determined by hydrogen adsorption and UV–vis spectroscopy, respectively [18,33]. These apparent contradictions to our findings can be explained by differences in catalyst preparation. In those studies [18,33], the alkali salts were added to the catalyst together with the precursor salt or prior to its impregnation. In contrast, the present work refers to a post synthesis modification similar to that reported by Yang et al. where iron-manganese catalysts promoted with potassium (Fe/Mn/K) were found to have larger hematite crystals than Fe/Mn catalysts [34].

XPS investigations of the chemical properties of both modified and unmodified catalysts revealed that the alkali modification shifted the $Fe2p_{3/2}$ band observed for the unmodified iron catalyst (711.29 eV) to slightly lower binding energy values (711.23 eV and 711.27 eV with rubidium and caesium, respectively). However these shifts are too small to imply significant changes in the chemical state of iron atoms. This suggests that (I) the alkali metal modification mainly affects the support and in turn (II) the support acid base functionality significantly influences the product distribution. The mean binding energy of the main line corresponded in all cases to those of ferric ions [35]. This result is in agreement with XRD studies of the same materials. Moreover a satellite band approximately 8 eV above the $Fe2p_{3/2}$, typical of α-Fe_2O_3 and γ-Fe_2O_3 [36], was distinguished (Fig. 11).

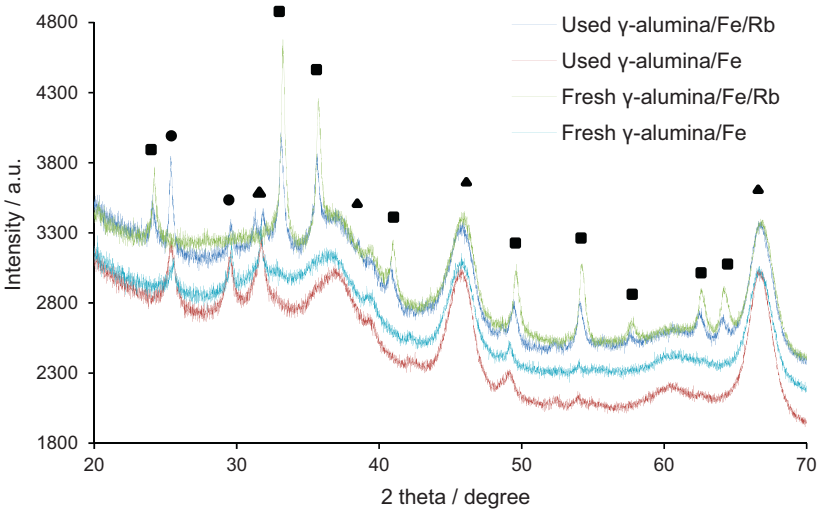

Fig. 10. X-ray diffraction patterns of alumina supported iron catalysts. (▲) γ-alumina, (■) hematite, (●) carbon.

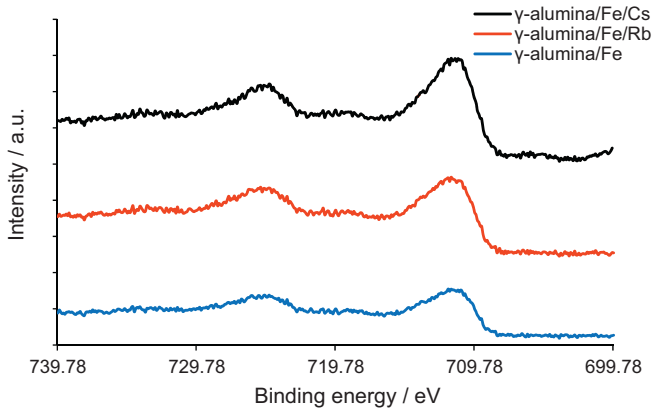

Fig. 11. Fe2p spectra of the γ-alumina/Fe, γ-alumina/Fe/Rb and γ-alumina/Fe/Cs catalysts.

The mean biding energies for $Rb3d_{5/2}$ and $Cs3d_{3/2}$ were found at 111.1 eV and 738.6 eV, respectively (Fig. 12). Note that the $Cs3d_{5/2}$ peak overlaps with the $Fe2p_{1/2}$ peak.

Fig. 13 shows the FTIR spectra of unmodified and modified catalysts under vacuum at room temperature. Bands at 1000 cm^{-1} are due to the Fe—OH bond and the band at 1600 cm^{-1} was assigned to the bending vibration of H—O—H^+ on the surface as previously reported [37] (both are spectral features characteristic of a hematite structure [38]). Differences at 1400 cm^{-1} between the unmodified and modified catalysts are due to the presence of rubidium nitrate [39]. Bands at 1350 cm^{-1} have been associated to the stretching mode of the nitrate ion [40]. The broad band with a maximum of ca 3500 cm^{-1} was assigned to OH stretching as reported for reactive aluminas [41].

3.5. Catalyst activity

Significant deactivation of the iron on alumina catalyst with time on stream was observed. Established causes of catalyst degradation include collapse of the support, coking, or active phase crystallite growth (reduction in dispersion) [42]. Neither abrasion nor induced crushing was experienced (mechanical), which suggests that, in the present study, the mechanism through which catalyst deactivation occurs is of a chemical nature (poisoning). Glycerol conversion was reduced by 20% after three hours of reaction over the unmodified catalyst, in comparison with a decrease of 10% following treatment with alkali salts (Fig. 14). These observations suggest that the caustic treatment poisons the acid sites that result in the formation of carbonaceous deposits on the catalyst during the reaction, and where condensation of glycerol, polymerisation of acrolein, side reactions between glycerol and acrolein [29] and condensation reactions between glycerol and formaldehyde [43] take place. The direct etherification of glycerol to form diglycerol and triglycerol was reported to take place over basic sites [44]. Under our conditions, despite the increased basicity due to the alkali modification of the catalyst,

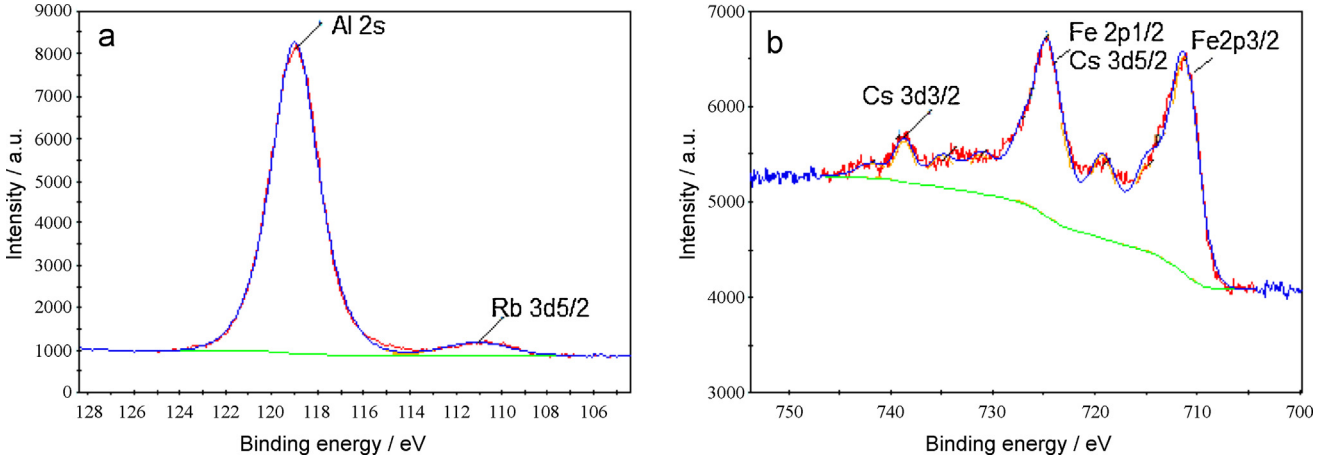

Fig. 12. (a) Rb3d/Al2s spectrum measured for γ-alumina/Fe/Rb. (b) Fe2p/Cs3d range spectrum measured for γ-alumina/Fe/Cs.

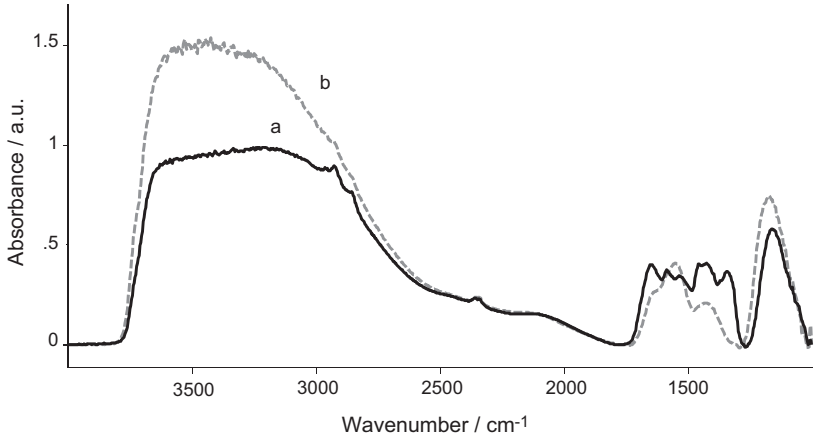

Fig. 13. FTIR spectra. (a) γ-Alumina/Fe/Rb. (b) γ-Alumina/Fe.

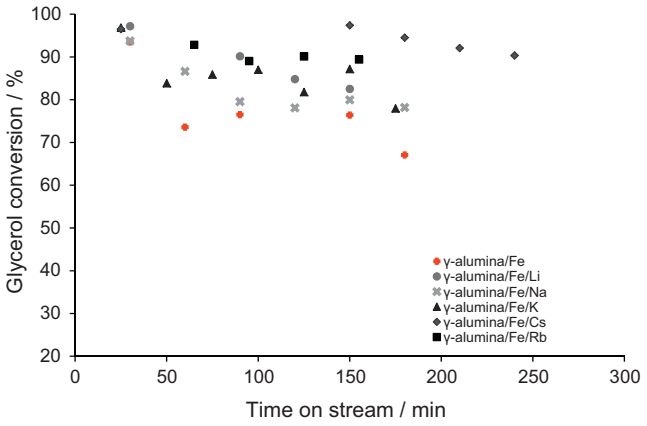

Fig. 14. Catalytic activity as a function of time on stream at 340 °C over different catalysts. Reactant: 35 wt% glycerol aqueous solution. GHSV = 1190 h^{-1}.

the conversion of glycerol differs in some ways from that reported in the study of Clacens et al. Most notably, our experiments were conducted in the gas phase whereas their etherification reaction was in the liquid phase. Other differences are the use of a solvent (water in 65 wt% the current experiments) and a higher reaction temperature in our catalytic measurements. These variables could have affected the formation of diglycerol and triglycerol. Chai et al. attributed the small rate of formation of polyglycerols to high temperatures with their experiments at 315 °C [45].

Deactivation mainly affects acrolein formation, substantiated by a reduction in the acrolein selectivity while the allyl alcohol yield remains virtually constant (Figs. 7b and 6a). These results are consistent with surface area measurements reported in Table 5. Moreover alkali metals have been reported to gasify carbonaceous deposits [46], which can explain their influence reducing catalyst deactivation under these conditions. Selection of the most suitable alkali metal for modifying the iron catalyst supported on alumina comprises its effect on enhancing the allyl alcohol route and the activity of the catalyst with time on stream. Despite the fact that over rubidium modified surfaces the allyl alcohol yield was higher, caesium exhibited less deactivation and lower acrolein formation.

Thermogravimetric studies conducted with used iron catalysts revealed an initial weight loss for both the unmodified and rubidium modified catalyst at low temperatures, associated to water removal (Fig. 15). Between 400 °C and 600 °C, the unmodified material had an apparent weight loss of approximately 7.5%, attributable to the removal of carbonaceous deposits. This behaviour was not observed in the course of weight loss for the rubidium modified catalyst. However, another mass change was observed for this sample at higher temperatures. Similar observations have been explained by the decomposition of rubidium compounds [18].

Post reactor studies were carried out in order to study the influence of alkali treatment on the catalytic functionality following regeneration and potential reutilisation of the catalyst system. Used lithium treated catalysts were reactivated by calcination at 400 °C in air flow for 4 h. Fig. 16 discloses a 10% decrease in conversion following regeneration, allyl alcohol yield is not fully re-established as a drop from 8.5% to 6.9% was observed. Catalyst deactivation was found to have small influence in the production of ally alcohol with time on stream, mainly affecting acrolein selectivity as shown in previous sections where alkali salts were not present in the catalyst surface. Interestingly, hydroxyacetone and ethanal production remained relatively constant following reactivation of the lithium modified iron material. Even though catalyst deactivation could not be completely overcome, regeneration in the presence of the alkali enhances glycerol conversion and selectivity towards allyl alcohol when comparing with the unmodified surface.

Studies to improve catalyst recyclability are being conducted in our laboratory through a variety of approaches. From a process point of view, it is possible to optimise certain conditions such as GHSV in order to reduce catalyst deactivation. In our experiments, a pronounced deactivation corresponds to an increase in the rate of acrolein formation. Acrolein can undergo an acid-catalysed polymerisation, as reported by Suprun et al. [29]. Under our reaction conditions, both acrolein production and catalyst deactivation increase at high GHSV which has been previously reported [47]. Therefore, optimising this parameter is important for catalyst stability, minimising the recurrence of reactivation. Another possibility to reduce coking is co-feeding hydrogen as studied before over catalysts doped with platinum group metals [48].

From a catalytic perspective, changes in the iron impregnation are to be implemented. In our experiments for longer reaction times (more than 48 h) a reduction of the iron content was observed in used catalysts.

For reactivation, instead of post reactor treatments, the feasibility of in situ regeneration is under assessment. This can be accomplished in cycles co-feeding air, either in the same reaction vessel or in a separate one, as described by Katryniok et al. [15].

3.6. Mechanistic considerations

Differences in product distribution obtained over both the iron catalysts and its support allowed a reaction pathway to be developed (Fig. 17).

Under our reaction conditions, glycerol undergoes dehydration which forms either formaldehyde/ethanal, acrolein or

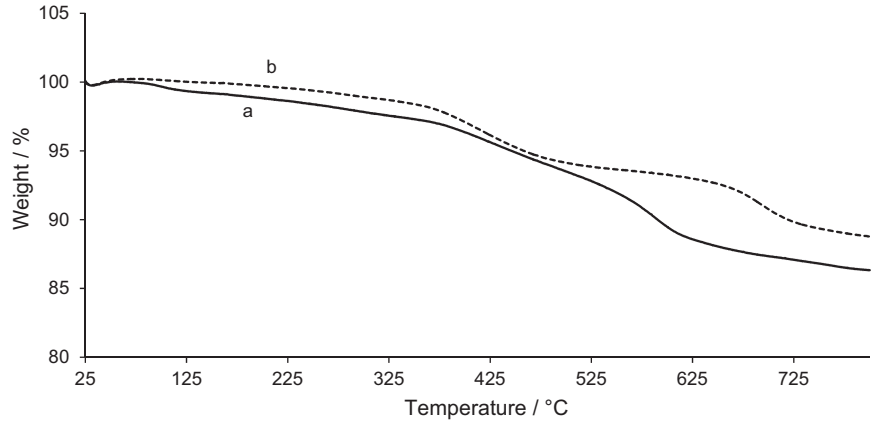

Fig. 15. Weight loss curves for used catalysts conducted on flowing nitrogen. (a) γ-Alumina/Fe. (b) γ-Alumina/Fe/Rb.

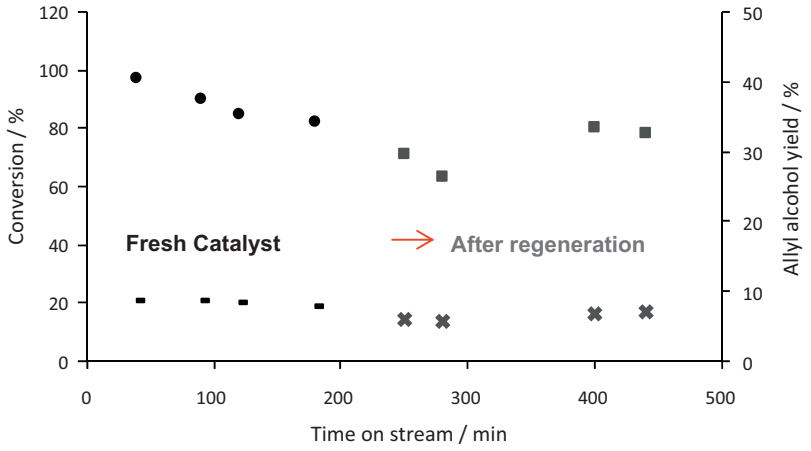

Fig. 16. Catalytic activity and allyl alcohol yield as a function of time on stream at 340 °C over lithium treated fresh and reactivated iron oxide on alumina catalysts. Reactant: 35 wt%. GHSV = 1190 h^{-1}.

1-hydroxyacetone as final products (determined by the position in the carbon chain where the dehydration reaction takes place [49]). Since the 1,3 dehydration of glycerol produces a carbon-carbon bond cleavage in the glycerol molecule, this pathway does not lead to allyl alcohol formation. Acrolein hydrogenation could take place in this system as reported before [9]. However, in our experiments acrolein production decreased over alkali metal modified catalysts by 3% absolute while an increase of 8% absolute in the yield of allyl alcohol was observed. Therefore, even if the total decrease in acrolein formation was the result of the carbonyl hydrogenation, more than 50% of the allyl alcohol would have had to be formed through another pathway.

Since the first pathway would hardly produce the desired alcohol and the second route does not entirely account for its formation in the observed yields, another allyl alcohol precursor could be species "b". The 1,2 dehydration of glycerol leading to species "b" (observed on surfaces of reduced acidity obtained by iron impregnation and alkali metal modification) is preferred over the 1,2 dehydration yielding product "e" and the subsequent acrolein formation. The later reaction takes place over the unmodified alumina, the surface with the highest acid site concentration as determined by TPD (refer to Section 3.3). Even though acidic sites are required for the initial dehydration of glycerol, significant quantities lead to product "e" instead of product "b" [50]. Basic sites have been reported to be detrimental to acrolein production, therefore, increasing its concentration through alkali metal deposition resulted in a reduced rate of acrolein formation [12].

Table 6
Gas phase composition in glycerol conversion over unmodified and rubidium modified iron catalysts.

Product	Concentration (vol%) over γ-alumina/Fe	Concentration (vol%) over γ-alumina/Fe/Rb
Carbon dioxide	2.87	3.23
Carbon monoxide	0.20	0.28
Hydrogen	0.46	0.63
Oxygen	0.46	0.22
Acrolein	1.48	1.45
Ethanal	1.43	1.47
Nitrogen	Balance	Balance

Alkali metals seem to have an effect favouring the formation of ethanal and formaldehyde from glycerol. The presence of alkali metals has been reported to influence the mechanism of formation of both species through the coordination of hydroxyl groups of glycerol by the alkali cation [51]. Formaldehyde is unstable at 340 °C and decomposes into hydrogen and carbon monoxide. The presence of higher quantities of both reducing agents (Table 6) could explain the enhanced yield of allyl alcohol through oxygen removal from

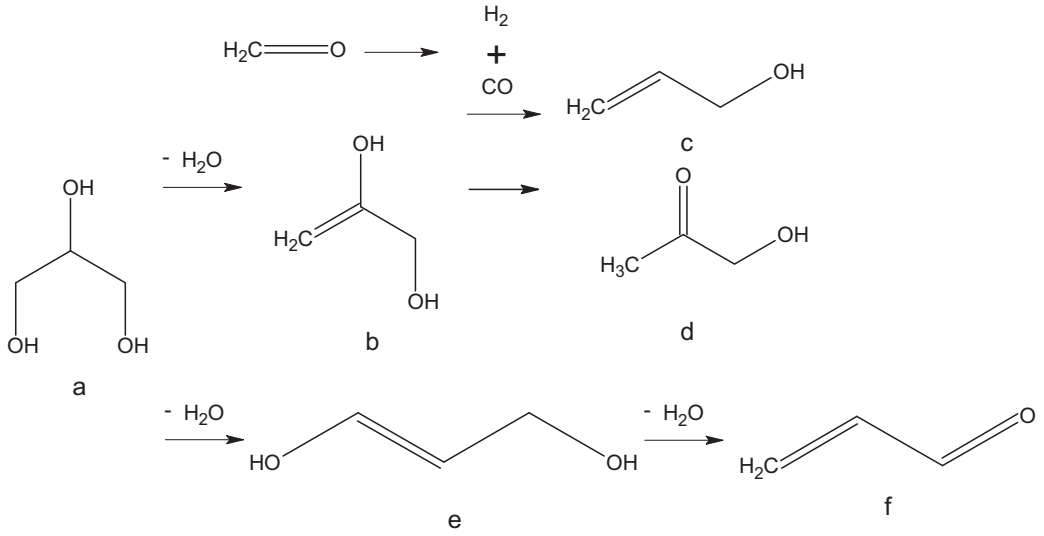

Fig. 17. Proposed reaction pathway.

intermediate "b". Iron plays an important role in providing redox sites for this reduction reaction to take place.

For the formation of allyl alcohol, two steps appear to be necessary. One is the dehydration reaction from glycerol to form intermediate "b" and the other is the redox site catalysed reduction of the intermediate "b". Increased reductant concentrations are expected to result in higher allyl alcohol yield at the expense of hydroxyacetone. Strong acidity (or a specific structure of sites such as paired sites) favours the single step 1,2 dehydration that leads to acrolein. Acrolein can then also form ethanal, which is a route for reductant formation over strongly acidic catalysts.

4. Conclusions

Iron catalysts were modified by alkali metal deposition and used in glycerol conversion. Alkali metal deposition techniques were assessed on the basis of allyl alcohol yield. Modification of the catalyst by caustic washing resulted in the most efficient treatment procedure. Temperature programmed desorption of isopropanol, ammonia and carbon dioxide confirmed changes in the acid–base properties of the iron catalyst due to alkali metal addition. Increases in basicity favoured allyl alcohol route and enhanced catalyst activity. A two-step process of allyl alcohol formation is suggested. Treatment resulted in reduction of acid sites, minimising acrolein production, and the poisoning of sites responsible for coke formation. An increase in surface area was observed in fresh catalysts in the presence of alkali metals with respect to the unmodified iron surface. Optimum allyl alcohol yield can be achieved by a subtle balance between acid, base and redox sites in the catalyst.

Acknowledgements

GS thanks the University of Newcastle for a post graduate research scholarship. Funding by African Explosives Ltd. is gratefully acknowledged. The authors thank the Electron Microscope and X-ray Unit of the University of Newcastle for the use of their facilities.

References

[1] D.Y.C. Leung, X. Wu, M.K.H. Leung, Applied Energy 87 (2010) 1083–1095.
[2] L. Bournay, D. Casanave, B. Delfort, G. Hillion, J.A. Chodorge, Catalysis Today 106 (2005) 190–192.
[3] X. Fan, R. Burton, Y. Zhou, The Open Fuels & Energy Science Journal 3 (2010) 17–22.
[4] M. Hájek, F. Skopal, Bioresource Technology 101 (2010) 3242–3245.
[5] F. Yang, M. Hanna, R. Sun, Biotechnology for Biofuels 5 (2012) 13.
[6] L. Liu, X.P. Ye, J.J. Bozell, ChemSusChem 5 (2012) 1162–1180.
[7] D.T. Johnson, K.A. Taconi, Environmental Progress 26 (2007) 338–348.
[8] Lyondell, Data Review and Assessment for Allyl Alcohol, 2005.
[9] Y. Liu, H. Tüysüz, C.-J. Jia, M. Schwickardi, R. Rinaldi, A.-H. Lu, W. Schmidt, F. Schüth, Chemical Communications 46 (2010) 1238–1240.
[10] T. Yoshikawa, T. Tago, A. Nakamura, A. Konaka, M. Mukaida, T. Masuda, Research on Chemical Intermediates 37 (2011) 1247–1256.
[11] E. Arceo, P. Marsden, R.G. Bergman, J.A. Ellman, Chemical Communications (2009) 3357–3359.
[12] Ü. Arda, Conversion of Glycerol to the Valuable Intermediates Acrolein and Allyl Alcohol in the Presence of Heterogeneous Catalysts, RWTH Aachen University, 2009, pp. 137.
[13] J. Yi, S. Liu, M.M. Abu-Omar, ChemSusChem 5 (2012) 1401–1404.
[14] C.J.A. Mota, B.P. Pinto, Current Physical Chemistry 2 (2012) 221.
[15] B. Katryniok, S. Paul, V. Belliere-Baca, P. Rey, F. Dumeignil, Green Chemistry 12 (2010) 2079–2098.
[16] B. Katryniok, S. Paul, M. Capron, F. Dumeignil, ChemSusChem 2 (2009) 719–730.
[17] P.O. Scokart, A. Amin, C. Defosse, P.G. Rouxhet, The Journal of Physical Chemistry 85 (1981) 1406–1412.
[18] B. Moens, H. De Winne, S. Corthals, H. Poelman, R. De Gryse, V. Meynen, P. Cool, B.F. Sels, P.A. Jacobs, Journal of Catalysis 247 (2007) 86–100.
[19] R. Fiedorow, I.G. Dalla Lana, The Journal of Physical Chemistry 84 (1980) 2779–2782.
[20] G. García Cortez, S.R. de Miguel, O.A. Scelza, A.A. Castro, Journal of Chemical Technology and Biotechnology 53 (1992) 177–180.
[21] S. Miguel, O. Scelza, A. Castro, J. Soria, Topics in Catalysis 1 (1994) 87–94.
[22] A. Konaka, T. Tago, T. Yoshikawa, A. Nakamura, T. Masuda, Applied Catalysis B: Environmental 146 (2014) 267–273.
[23] G. Sanchez, L. Harvey, J. Friggieri, B.Z. Dlugogorski, E. Kennedy, M. Stockenhuber, 17th International Zeolite Conference, Russia, 2013.
[24] M. Hájek, F. Skopal, J. Kwiecien, M. Černoch, Talanta 82 (2010) 283–285.
[25] A.H. Hazimah, T.L. Ooi, A. Salmiah, Journal of Oil Palm Research 15 (2003) 1–5.
[26] M.L.M. Bonati, R.W. Joyner, M. Stockenhuber, Catalysis Today 81 (2003) 653–658.
[27] K.D. Pathak, Catalytic Conversion of Glycerol to Value-Added Liquid Chemicals, Department of Chemical Engineering, University of Saskatchewan, 2005, pp. 150.
[28] M.H. Haider, N.F. Dummer, D. Zhang, P. Miedziak, T.E. Davies, S.H. Taylor, D.J. Willock, D.W. Knight, D. Chadwick, G.J. Hutchings, Journal of Catalysis 286 (2012) 206–213.
[29] W. Suprun, M. Lutecki, T. Haber, H. Papp, Journal of Molecular Catalysis A: Chemical 309 (2009) 71–78.
[30] M. Mohapatra, S. Anand, International Journal of Engineering, Science and Technology 2 (2010) 127–146.
[31] M. Stockenhuber, G. Sanchez, J. Friggieri, C. Keast, L. Harvey, B.Z. Dlugogorski, E. Kennedy, 15th International Catalysis Conference, Germany, 2012.
[32] K.S. Walton, M.B. Abney, M. Douglas LeVan, Microporous and Mesoporous Materials 91 (2006) 78–84.
[33] J. Haber, M. Nattich, T. Machej, Applied Catalysis B: Environmental 77 (2008) 278–283.
[34] Y. Yang, H.-W. Xiang, Y.-Y. Xu, L. Bai, Y.-W. Li, Applied Catalysis A: General 266 (2004) 181–194.
[35] N.S. McIntyre, D.G. Zetaruk, Analytical Chemistry 49 (1977) 1521–1529.
[36] A.P. Grosvenor, B.A. Kobe, M.C. Biesinger, N.S. McIntyre, Surface and Interface Analysis 36 (2004) 1564–1574.
[37] J.M. Fang, S.H. Li, W.Q. Gong, Z.Y. Sun, H.G. Yang, Spectroscopy and Spectral Analysis (2) (2009) 318–321.
[38] R.M. Cornell, U. Schwertmann, The Iron Oxides. Structure, Properties, Reactions, Occurrence and Uses, 2nd ed., 2003.
[39] E. Mayer, Spectrochimica Acta Part A: Molecular Spectroscopy 42 (1986) 1277–1279.
[40] D.J. Goebbert, E. Garand, T. Wende, R. Bergmann, G. Meijer, K.R. Asmis, D.M. Neumark, The Journal of Physical Chemistry A 113 (2009) 7584–7592.
[41] J. Ryczkowski, Catalysis Today 68 (2001) 263–381.
[42] C.H. Bartholomew, Applied Catalysis A: General 212 (2001) 17–60.
[43] J. Deutsch, A. Martin, H. Lieske, Journal of Catalysis 245 (2007) 428–435.
[44] J.M. Clacens, Y. Pouilloux, J. Barrault, Applied Catalysis A: General 227 (2002) 181–190.
[45] S.-H. Chai, H.-P. Wang, Y. Liang, B.-Q. Xu, Green Chemistry 9 (2007) 1130–1136.
[46] G.R. Meima, P.G. Menon, Applied Catalysis A: General 212 (2001) 239–245.
[47] C.-J. Jia, Y. Liu, W. Schmidt, A.-H. Lu, F. Schüth, Journal of Catalysis 269 (2010) 71–79.
[48] A. Alhanash, E.F. Kozhevnikova, I.V. Kozhevnikov, Applied Catalysis A: General 378 (2010) 11–18.
[49] M.R. Nimlos, S.J. Blanksby, X. Qian, M.E. Himmel, D.K. Johnson, The Journal of Physical Chemistry A 110 (2006) 6145–6156.
[50] A.K. Kinage, P.P. Upare, P. Kasinathan, Y.K. Hwang, J.-S. Chang, Catalysis Communications 11 (2010) 620–623.
[51] J.B. Paine III, Y.B. Pithawalla, J.D. Naworal, C.E. Thomas Jr., Journal of Analytical and Applied Pyrolysis 80 (2007) 297–311.